Stator-Current Spectrum Signature of Healthy Cage Rotor Induction Machines

Gojko M. Joksimović, *Senior Member, IEEE*, Jakša Riger, Thomas M. Wolbank, *Member, IEEE*, Nedjeljko Perić, *Senior Member, IEEE*, and Mario Vašak, *Member, IEEE*

***Abstract*—Before applying current-signature-analysis-based monitoring methods, it is necessary to thoroughly analyze the existence of the various harmonics on healthy machines. As such an analysis is only done in very few papers, the objective of this paper is to make a clear and rigorous characterization and classification of the harmonics present in a healthy cage rotor induction motor spectrum as a starting point for diagnosis. Magnetomotive force space harmonics, slot permeance harmonics, and saturation of main magnetic flux path through the virtual air-gap permeance variation are taken into analytical consideration. General rules are introduced giving a connection between the number of stator slots, rotor bars, and pole pairs and the existence of rotor slot harmonics as well as saturation-related harmonics in the current spectrum. For certain combinations of stator and rotor slots, saturation-related harmonics are shown to be most prominent in motors with a pole pair number of two or more. A comparison of predicted and measured current harmonics is given for several motors with different numbers of pole pairs, stator slots, and rotor bars.**

***Index Terms*—Condition monitoring, fault detection, fault diagnosis, Fourier transforms, induction machines, induction motor drives, preventive maintenance, spectrum analysis.**

NOMENCLATURE

B	Magnetic flux density (in teslas).
F	Frequency (in hertz).
f_1	Fundamental frequency (in hertz).
f_{L_PSH}	Lower principal slot harmonic (PSH) frequency (in hertz).
f_{U_PSH}	Upper PSH frequency (in hertz).
f_{L_RSH}	Lower rotor slot harmonic (RSH) frequency (in hertz).
f_{U_RSH}	Upper RSH frequency (in hertz).
f_{L_SH}	Lower saturation-related harmonic frequency (in hertz).
f_{U_SH}	Upper saturation-related harmonic frequency (in hertz).
g	Ordinal number.
g_0	Air-gap length (in meters).
k	Ordinal number.
k_m	Saturation factor 1.
k_{sat}	Saturation factor 2.
M	Magnetomotive force (MMF) (in amperes).
n	Ordinal number.
p	Pole pair number.
P	Permeance (in 1/m).
R	Number of rotor slots (bars).
S	Number of stator slots.
s	Slip.
s_ν	Slip for νth harmonic.
t	Time (in seconds).
U_{sat}	Voltage in saturated machine (in volts).
$U_{\mathrm{non\_sat}}$	Voltage in nonsaturated machine (in volts).
β	Angular position of air-gap flux (in electrical radians).
ν	Harmonic order.
ω	Angular frequency (in radians per second).
λ	Harmonic order.
θ_r	Angle measured in rotor reference frame (in radians).
θ_s	Angle measured in stator reference frame (in radians).

Manuscript received April 12, 2012; revised July 19, 2012 and November 4, 2012; accepted December 13, 2012. Date of publication January 4, 2013; date of current version May 2, 2013. This work was supported by the European Commission and Montenegro under Grant FP7-SEE-ERA.net PLUS ERA 80/01.

G. M. Joksimović and J. Riger are with the Faculty of Electrical Engineering, University of Montenegro, 81000 Podgorica, Montenegro (e-mail: joxo@ac.me; jaksa@ac.me).

T. M. Wolbank is with the Institute of Energy Systems and Electrical Drives, Department of Electrical Drives and Machines, Vienna University of Technology, 1040 Vienna, Austria (e-mail: thomas.wolbank@tuwien.ac.at).

N. Perić and M. Vašak are with the Faculty of Electrical Engineering and Computing (FER), University of Zagreb (UNIZG), 10000 Zagreb, Croatia (e-mail: nedjeljko.peric@fer.hr; mario.vasak@fer.hr).

Color versions of one or more of the figures in this paper are available online at http://ieeexplore.ieee.org.

Digital Object Identifier 10.1109/TIE.2012.2236995

I. INTRODUCTION

ONLINE condition monitoring has become a very important issue in safety critical systems. Condition monitoring can significantly improve reliability and enable timely planning of repairs, particularly when it comes to high-power machines, i.e., high-price machines or machines that are important prime movers for complex systems.

Electrical machines and drive systems are subject to many different types of faults. These faults include the following [1].

1) Stator winding faults [2]–[4].
2) Rotor electrical faults (e.g., broken rotor bar, cracked end ring, or short circuit in case of wound rotor machines) [2], [5]–[7].
3) Rotor mechanical faults (e.g., bearing damage, eccentricity, bent shaft, and misalignment) [8]–[13].
4) Failure of one or more power electronic components of the drive system [14], [15]. In order to monitor the machine's health condition and to make online diagnosis, many different techniques have been developed. Among others, one can mention the measurement and spectral analysis of the axial magnetic flux by using the

search coil, temperature measurement, infrared recognition, noise and vibration monitoring, motor-current signature analysis (MCSA), etc. [16].

Among the mentioned techniques, MCSA has particularly significant importance. Stator line current frequency spectrum represents, a sort of speaking, an electrocardiogram of electrical machine. This technique is particularly useful because it is noninvasive, and search coil is the machine stator winding itself.

Although MCSA is one of the most powerful methods for diagnosing motor faults, it has some shortcomings.

1) MCSA requires high precision of slip-frequency information.
2) Stator-current data should be sampled after motor speed arrives at the steady state.
3) Unspecified harmonic numbers induce ambiguous results from MCSA-based diagnosis methods [17].

In order to make the correct interpretation of changes in the spectrum as a result of different faulty regimes, one should be familiar with the current spectrum of the healthy machine [18], which is not an easy task because of the complexity of electromagnetic processes, variable in space and time, which occur in the machine. In other words, it is necessary to have a powerful mathematical model that enables numerical modeling of the machine taking into account exact geometrical representation of the machine. Such a model that is widely recognized as very powerful tool for modeling and analysis of different faults in induction machines is based on winding function approach [19].

To get a deeper insight into the origin of the different current harmonics, an appropriate analytical model has to be used in addition to the numerical one. The most common approach for these purposes is the MMF–permeance wave approach. There, the magnetic flux density waves in the air gap are obtained from multiplication of MMF and permeance wave [8]. The application of both models, numerical and analytical, verified by measurements, allows to draw conclusions on the order and magnitude of fault-induced current harmonics.

In the literature, induction machines are usually modeled assuming smooth air gap. As a result, only a small number of papers are taking into account also stator and rotor slotting as possible source of harmonics in the stator-current spectrum [10], [19], [20].

A further simplification usually applied is the assumption of infinite permeability of the iron core which results in all magnetic machine properties being defined by the air gap only. Keeping the stator-current spectrum of a real machine in mind, this simplification is not able to describe the harmonics introduced or influenced by saturation of the main flux path.

A model to investigate the influence of saturation along the magnetic flux path was presented in [21]. There, new saturation-related frequency components in stator-current spectrum were deduced.

The objective of this paper is to make a clear and rigorous characterization and classification of all harmonics present in a healthy cage rotor induction motor spectrum as a starting point for diagnosis.

In the first part of this paper, a short overview on the MMF space harmonics is given. This part of this paper introduces general rules that describe the connection between the number of stator slots, rotor bars, and pole pairs and the existence of RSHs in stator-current spectrum.

The second part of this paper deals with slot permeance harmonics. As will be shown, certain combinations of stator, rotor slot, and pole pair number have a significant influence on the magnitude of stator-current harmonics at RSH frequencies.

Finally, the third part deals with saturation of the main magnetic flux path in the machine and its influence on the existence of saturation-related current harmonics.

In addition, the properties of the third-harmonic current component which is always more or less pronounced are explained.

Stator-current harmonics analytically predicted are validated in the last part of this paper through experimental spectra of three different machines as well as spectra of a fourth machine, taken from open literature.

II. Space MMF Harmonics

Due to the placement of the three-phase stator winding in slots, the phase as well as the resultant rotating MMF wave shape is stepwise. Therefore, rotating MMF beside the fundamental harmonic with p pole pairs also contains higher space harmonics. The aforementioned series of MMF space harmonics is defined by the well-known expression

$$\nu = 6g + 1, \qquad g = 0, \pm 1, \pm 2, \ldots \tag{1}$$

where ν is harmonic order. Aside from the fifth and seventh space harmonics, which are a consequence of trapezoidal phase MMF shape, stator slot harmonics are two of the most prominent higher space harmonics in the stepwise MMF waveform. Their existence is, in accordance with the definition of MMF, a result of current flowing through the corresponding winding and a consequence of the discrete nature of the stator windings, i.e., conductor placement in the slots.

For a stator with S slots, in a machine with p pole pairs, slot harmonics are of order $\lambda S/p \pm 1,\ \lambda = 1, 2, \ldots$. These harmonics belong to the series of the higher MMF space harmonics generated by a symmetrical three-phase stator winding supplied by a system of symmetrical three-phase voltages (1). In such a series, they are, for $\lambda = 1$, the most prominent space harmonics in the spectrum, and it is well known that these harmonics are not able to be attenuated using short-pitched stator windings [22].

RSHs are of much more interest in cage induction motors and not only are the most prominent space harmonics of rotor MMF but also exist only in the spectrum beside the fundamental rotor MMF wave. Rotor cage reacts on the flux density waves from stator side with the following three series of MMF waves [23]:

$$M_1 = M_{1m} \cos(s_\nu \omega t - \nu p \theta_r) \tag{2}$$

$$M_2 = M_{2m} \cos\left(s_\nu \omega t + \left(\frac{\lambda R}{p} - \nu\right) p\theta_r\right) \tag{3}$$

$$M_3 = M_{3m} \cos\left(s_\nu \omega t - \left(\frac{\lambda R}{p} + \nu\right) p\theta_r\right) \tag{4}$$

where s_ν is slip of MMF νth-order harmonic

$$s_\nu = 1 - \nu(1-s). \tag{5}$$

In a nonsaturated machine, these MMF waves interact with the constant air-gap permeance (neglecting stator and rotor slotting), producing the same shape of flux density waves. These waves, now in the stator frame of reference, are

$$B_1 = B_{1m}\cos(\omega t - \nu p\theta_s) \tag{6}$$

$$B_2 = B_{2m}\cos\left(\left(1-\lambda\frac{R}{p}(1-s)\right)\omega t + \left(\frac{\lambda R}{p}-\nu\right)p\theta_s\right) \tag{7}$$

$$B_3 = B_{3m}\cos\left(\left(1+\lambda\frac{R}{p}(1-s)\right)\omega t - \left(\frac{\lambda R}{p}+\nu\right)p\theta_s\right). \tag{8}$$

Therefore, all of the flux density space harmonics from the stator side rotor reflect at the fundamental frequency and a series of two additional slip-dependent frequencies, located rather high in the stator-current spectrum, that are known as the RSHs, lower

$$f_{L\_\mathrm{RSH}} = \left(1 - \lambda\frac{R}{p}(1-s)\right) f_1 \tag{9}$$

and upper

$$f_{U\_\mathrm{RSH}} = \left(1 + \lambda\frac{R}{p}(1-s)\right) f_1 \tag{10}$$

where $\lambda = 1, 2, 3, \ldots$. For $\lambda = 1$, one has the first-order RSH or PSHs. These flux density waves induce electromotive forces (EMFs) and lead to currents in the stator windings at the same frequencies.

Obviously, frequencies given by (9) and (10) depend on machine load, i.e., slip. By other words, position of PSH in stator-current spectrum depends on rotor speed. That is what makes them interesting and is the reason why these harmonics have found wide application in the sensorless speed estimation of induction motor drives using numerous different techniques for digital signal processing [24]–[26].

However, the existence of stator-current components at frequencies given by (9) and (10) depends on the number of pole pairs in the flux density waves in(7) and (8). In order that spectral component at the lower PSH frequency (9) exists in the stator-current spectrum, it is required that the number of pole pairs in the flux density wave (7) is equal to the number of pole pairs produced by the stator winding itself. In other words, $R/p - \nu$ for some adequate value of $\nu(1)$ must belong to the group $\mathbf{H} = (6k+1)$. It further means that

$$R_{L\_\mathrm{PSH}} = p\left[6(g+k)+2\right], \quad g = 0, \pm1, \pm2, \ldots; \qquad k = 0, \pm1, \pm2, \ldots. \tag{11}$$

It can be easily concluded from (11) that, for a rotor with R bars, in a p pole pair motor

$$R_{L\_\mathrm{PSH}} = (6n+2)p, \qquad n = 0, 1, 2, 3, \ldots \tag{12}$$

lower PSH in the stator-current spectrum will exist. In case of a four-pole machine, $R_{L\_\mathrm{PSH}} = 4, 16, 28, 40, \ldots$.

On the other hand, the condition for the existence of the upper PSH is satisfied for rotors with the following number of bars:

$$R_{U\_\mathrm{PSH}} = -p\left[6(g+k)+2\right], \quad g = 0, \pm1, \pm2, \ldots; \qquad k = 0, \pm1, \pm2 \tag{13}$$

which is equivalent to the following expression:

$$R_{U\_\mathrm{PSH}} = (6n-2)p, \qquad n = 1, 2, 3, \ldots. \tag{14}$$

This leads to $R_{U\_\mathrm{PSH}} = 8, 20, 32, 44, \ldots$ for a four-pole machine.

In order that both PSHs exist in the stator-current spectrum, the number of rotor bars in p pole pair motor must be equal to the mean value of (12) and (14)

$$R_{\mathrm{BOTH\_PSH}} = 6np, \qquad n = 1, 2, 3, \ldots. \tag{15}$$

This leads to the well-known "forbidden" combinations of stator and rotor slot numbers [22] ($R_{\mathrm{BOTH\_PSH}} = 12, 24, 36, 48, \ldots$ for a four-pole motor). Rotors with R bars in p pole pair symmetrical induction motor, which do not satisfy any of conditions (12), (14), and (15), will not have any PSHs in the stator-current spectrum, under symmetrical voltage supply conditions.

III. Slot Permeance Harmonics

Aside from the described stator or rotor MMF space harmonics, another effect exists in a real induction motor which generates EMFs and currents in stator windings at the same frequencies given by (9) and (10), as explained as follows. This is the stator and rotor slotting effect, i.e., the air-gap length that varies with both space and time as a function of rotation of the rotor. As stated previously, both MMF space harmonics and slot permeance harmonics induce EMFs and lead to the stator currents at the same frequencies. Hence, the distinction between the contributions of these components is blurred. The main differentiation between these two effects is that rotor MMF space harmonics exist only in case when current flows through the cage winding, even in the no-load case. This is as a consequence of high-frequency rotor currents induced by rotating flux density wave harmonics from the stator side. For the existence of rotor permeance slot harmonics, this precondition is not needed. Even a slotted rotor without any winding, rotating in the motor by some external means, e.g., an auxiliary motor, will lead to stator winding current components at frequencies given by (9) and (10) if the stator winding is connected to the voltage supply. In this case, the slip in (9) and (10) is simply the difference between the synchronous speed and the speed of the auxiliary motor. The reason for the existence of these stator-current components is that the self-inductance of the stator windings becomes a function of time as a consequence of variable permeance due to the changing rotor angle.

The actual induction motor air-gap permeance is variable in both space and time as a consequence of stator and rotor slotting and their mutual position as a function of rotor angle.

Taking into account only the fundamental harmonic of air-gap permeance series, the air-gap permeance function is commonly described by the following series [19]:

$$P(\theta_s,\theta_r)=\frac{1}{g_0}+P_s\cos(S\theta_s)+P_r\cos(R\theta_r)+P_{sr}\cos(S\theta_s-R\theta_r)+\cdots \quad (16)$$

where coefficients $P_s, P_r,$ and P_{sr} depend on the geometrical dimensions of the air gap and stator and rotor slot opening. The situation when stator MMF waves given by

$$M_{s\nu}(t,\theta_s)=M_{s\nu\,\max}\cos(\omega t-\nu p\theta_s) \quad (17)$$

act on the third term of (16) is considered next. As a result, two flux density waves are obtained, expressed in the stator frame of reference as

$$B_{s\nu1}(t,\theta_s)=B_{s\nu1\,\max}\cos\left(\left(1-\frac{R}{p}(1-s)\right)\omega t+\left(\frac{R}{p}-\nu\right)p\theta_s\right) \quad (18)$$

$$B_{s\nu2}(t,\theta_s)=B_{s\nu2\,\max}\cos\left(\left(1+\frac{R}{p}(1-s)\right)\omega t-\left(\frac{R}{p}+\nu\right)p\theta_s\right) \quad (19)$$

which are identical with waves (7) and (8).

On the other side, stator MMF waves (17) acting on the fourth term in the permeance expression (16) lead to flux density waves of the same frequencies but with different number of pole pairs given by

$$B_{s\nu3}(t,\theta_s)=B_{s\nu3\,\max}\cos\left(\left(1-\frac{R}{p}(1-s)\right)\omega t-\left(\frac{S-R}{p}+\nu\right)p\theta_s\right) \quad (20)$$

$$B_{s\nu4}(t,\theta_s)=B_{s\nu4\,\max}\cos\left(\left(1+\frac{R}{p}(1-s)\right)\omega t+\left(\frac{S-R}{p}-\nu\right)p\theta_s\right). \quad (21)$$

As will be shown, this difference in pole pair number (at certain combination of stator, rotor slot, and pole pair number) can have a significant influence on stator-current component's amplitudes at these frequencies.

IV. Saturation Permeance Harmonics

The saturation of the main magnetic flux path in a machine can be modeled by making the air-gap length a function of the saturation level and spatial position (Fig. 1). In this approach, the maximum value of the virtual air-gap length corresponds to the maxima/minima of the main magnetic flux density wave, while the minimum value of the virtual air-gap length (equal to the effective value of the air-gap length) corresponds to the zero value of the main magnetic flux density wave.

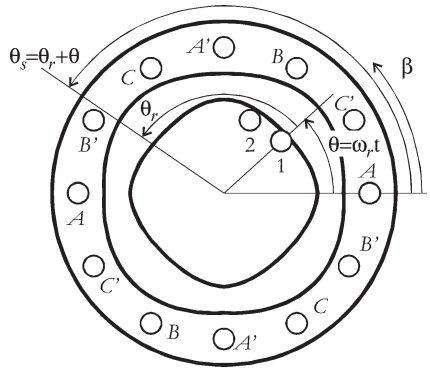

Fig. 1. Virtual air-gap length variation along the machine circumference due to the main magnetic flux path saturation, $p=2$, $\beta=\pi/2$ rad.

Accordingly, the air-gap permeance function, neglecting the stator and rotor slotting, is described with the following expression [27]:

$$P(\theta_s,\beta)=\frac{1}{g_0}-k_m-k_m\cos(2p\theta_s-2\beta) \quad (22)$$

where g_0 is the effective air-gap length and p is the machine's number of pole pairs.

Angle θ_s (in mechanical radians) defines position along the stator circumference, while β (in electrical radians) describes the angular position of the air-gap flux density maximum in the stator frame of reference. The factor k_m is correlated with the saturation factor in the following manner. Product of the permeance function and the fundamental MMF wave $M_{1\,\max}\cos(\omega t-p\theta_s)$ gives two flux density waves

$$B(t,\theta_s)=M_{1\,\max}\left(\frac{1}{g_0}-\frac{3}{2}k_m\right)\cos(\omega t-p\theta_s)-M_{1\,\max}\frac{k_m}{2}\cos(3\omega t-3p\theta_s). \quad (23)$$

The maximum value of the fundamental flux density wave in (23) should correspond to the saturated condition of the machine ($B_{\rm sat}\sim E_{\rm sat}\sim U_{\rm sat}$). In unsaturated machine, the maximal value of the fundamental flux density wave ($B_{\rm non\_sat}\sim E_{\rm non\_sat}\sim U_{\rm non\_sat}$) should correspond to the inverse value of the effective air-gap length, i.e.,

$$\frac{1}{g_0}:U_{\rm non\_sat}=\left(\frac{1}{g_0}-\frac{3}{2}k_m\right):U_{\rm sat}. \quad (24)$$

As the saturation factor is the ratio of the fundamental components of the air-gap voltage in unsaturated and saturated conditions

$$k_{\rm sat}=\frac{U_{\rm non\_sat}}{U_{\rm sat}} \quad (25)$$

previous relationship results in

$$k_m=\frac{2}{3}\frac{1}{g_0}\frac{k_{\rm sat}-1}{k_{\rm sat}}. \quad (26)$$

The air-gap permeance function (22) now attains a compact form

$$P = P_1 + P_2 = P_1 + P_{2m}\cos(2p\theta_s - 2\beta) \tag{27}$$

where

$$P_1 = \frac{1}{g_0}\left(1 - \frac{2}{3}\frac{k_{\rm sat}-1}{k_{\rm sat}}\right) \tag{28}$$

$$P_{2m} = -\frac{2}{3}\frac{1}{g_0}\frac{k_{\rm sat}-1}{k_{\rm sat}}. \tag{29}$$

Symmetrical three-phase stator winding produces a series of MMF waves, described by the well-known relation

$$M_s = M_{sm}\cos(\omega t - \nu p\theta_s) \tag{30}$$

where $\nu = 6g+1$, $g = 0, \pm1, \pm2, \ldots$. These waves, in interaction with the air-gap permeance function (27), produce a numerous magnetic flux density waves. It should be noted that, in a steady-state condition, $\beta = \omega t$.

In a saturated machine, two different effects can be noticed. First of all, rotor MMF waves (2)–(4) experience a variable air-gap permeance. In interaction with P_2(27), rotor MMF waves produce the following flux density waves, in stator reference frame:

$$B_{11\rm sat} = B_{11m\rm sat}\cos\left(\omega t + (\nu-2)p\theta_s\right) \tag{31}$$

$$B_{12\rm sat} = B_{12m\rm sat}\cos\left(3\omega t - (\nu+2)p\theta_s\right) \tag{32}$$

$$B_{21\rm sat} = B_{21m\rm sat}\cos\left(\left(1+\lambda\frac{R}{p}(1-s)\right)\omega t - \left(\frac{\lambda R}{p} - (\nu-2)\right)p\theta_s\right) \tag{33}$$

$$B_{22\rm sat} = B_{22m\rm sat}\cos\left(\left(3-\lambda\frac{R}{p}(1-s)\right)\omega t + \left(\frac{\lambda R}{p} - (\nu+2)\right)p\theta_s\right) \tag{34}$$

$$B_{31\rm sat} = B_{31m\rm sat}\cos\left(\left(1-\lambda\frac{R}{p}(1-s)\right)\omega t + \left(\frac{\lambda R}{p} + (\nu-2)\right)p\theta_s\right) \tag{35}$$

$$B_{32\rm sat} = B_{32m\rm sat}\cos\left(\left(3+\lambda\frac{R}{p}(1-s)\right)\omega t - \left(\frac{\lambda R}{p} + (\nu+2)\right)p\theta_s\right). \tag{36}$$

As the pole pair number in (32) is a multiple of three for any value of ν, the third-harmonic component in stator-current spectrum cannot arise in a symmetrical machine connected to balanced three-phase voltages.

Second, stator MMF waves in a saturated induction machine, through variable air-gap permeance P_2, induce flux density waves that do not exist in an unsaturated machine. These waves are

$$B_4 = B_{4m}\cos\left((1-(2-\nu)(1-s))\,\omega t + (\nu-2)p\theta_r\right) \tag{37}$$

$$B_5 = B_{5m}\cos\left((3-(\nu+2)(1-s))\,\omega t - (\nu+2)p\theta_r\right). \tag{38}$$

Due to these waves, new MMF waves in the cage rotor can appear. However, these new MMF waves, in the previously described manner, can induce the EMFs and lead to currents in the stator winding only at the same frequencies as in (31)–(36). Hence, in a saturated induction machine, new stator-current components can be expected only at the following frequencies: lower saturation-related harmonic (L_SH)

$$f_{L\_\rm SH} = \left(3 - \lambda\frac{R}{p}(1-s)\right)f_1 \tag{39}$$

and upper saturation-related harmonic (U_SH)

$$f_{U\_\rm SH} = \left(3 + \lambda\frac{R}{p}(1-s)\right)f_1. \tag{40}$$

Similarly, as for the PSHs, in order that stator-current components arise at frequencies given by (39), the number of pole pairs of the magnetic flux density waves (34) must be the same as the number of pole pairs that the stator winding itself produces. This means that, in order that stator-current component at the lower saturation-related frequency exists, $R/p - (\nu+2)$ must belong to group $\mathbf{H} = (6k+1)$, where $k = 0, \pm1, \pm2, \ldots$.

The same condition holds for the upper saturation-related PSH.

V. Stator-Current Spectrum Content

According to the previously derived rules for the existence of different harmonics in stator-current spectrum, it is an easy task to form an algorithm that can decide which of the harmonics in the stator-current spectrum for different numbers of p, S, and R exist and what their relative intensity is.

Thus, the following table can be formed for the most common combinations of stator and rotor slots for cage rotor induction machines.

The following consideration explains the notation in the table (e.g.,"big big").

Considering a motor with $p = 2$, $S = 36$ stator slots, and $R = 44$ rotor bars, stator slot harmonics are of order $S/p \pm 1$, i.e., -17th and $+19$th. In order that the lower saturation-related harmonic (L_SH) appears in stator-current spectrum, $R/p - (\nu+2)$ should belong to the $\mathbf{H} = (6k+1)$ group, where $k = 0, \pm1, \pm2, \ldots$.

For $\nu = 1$, $R/p - (\nu+2) = 44/2 - 3 = 19$, i.e., for the most significant harmonic from stator side, the result is also a significant harmonic equal to the upper stator slot harmonic (first big in table). On the other side, for $\nu = 19$, $R/p - (\nu+2) = 44/2 - 21 = 1$, i.e., for a relatively big harmonic from the stator side, the upper stator slot harmonic results in a fundamental harmonic (second big)! Therefore, it can be expected that L_SH in the stator-current spectrum of this machine will be rather prominent as it will be shown later.

Consider another machine with $p = 4$ pole pairs, $S = 48$ stator slots, and $R = 64$ rotor bars. For this motor, stator slot harmonics are of order $S/p \pm 1$, i.e., -11th and $+13$th. In order that the lower saturation-related harmonic (L_SH) appears in stator-current spectrum, $R/p - (\nu+2)$ should belong to the $\mathbf{H} = (6k+1)$ group, where $k = 0, \pm1, \pm2, \ldots$.

TABLE I
EXISTENCE AND RELATIVE SIZE OF HARMONICS IN STATOR-CURRENT SPECTRUM FOR DIFFERENT POLE PAIR NUMBERS AND DIFFERENT STATOR/ROTOR SLOT NUMBERS

TWO POLE (p=1) CAGE ROTOR INDUCTION MACHINE				
S/R	L_SH	L_PSH	U_PSH	U_SH
24/18	small	small	small	small
24/32	small	small	/	small
36/28	small	/	small	small
48/40	small	/	small	small
FOUR POLE (p=2) CAGE ROTOR INDUCTION MACHINE				
S/R	L_SH	L_PSH	U_PSH	U_SH
36/28	small	small	/	**big**
36/32	small	/	**big big**	**big**
36/44	**big big**	/	small	small
36/45	/	/	/	/
48/40	small	small	/	**big**
60/47	/	/	/	/
60/73	/	/	/	/
72/58	/	/	/	/
SIX POLE (p=3) CAGE ROTOR INDUCTION MACHINE				
S/R	L_SH	L_PSH	U_PSH	U_SH
36/45	/	/	/	/
54/42	small	small	/	**big**
72/60	small	small	/	**big**
90/71	/	/	/	/
EIGHT POLE (p=4) CAGE ROTOR INDUCTION MACHINE				
S/R	L_SH	L_PSH	U_PSH	U_SH
36/52	/	/	/	/
48/64	**big big**	/	small	small
72/56	small	small	/	**big**
72/89	/	/	/	/
96/80	small	small	/	**big**

For $\nu = 1$, $R/p - (\nu + 2) = 64/4 - 3 = 13$, i.e., for the most significant harmonic from stator side, the result is also a significant harmonic equal to stator slot harmonic (first big in table). On the other side, when $\nu = 13$, $R/p - (\nu + 2) = 64/4 - 15 = 1$, i.e., for relatively big harmonic from stator side, the stator slot harmonic results in a fundamental harmonic (second big). Therefore, L_SH in the stator-current spectrum of this machine will be rather prominent (big big).

It is, however, also possible that a machine does not produce any of the analyzed stator-current harmonics. These configurations exist when the number of rotor slots is odd, because, in that case, quotient R/p is not an integer.

In addition, machines exist with an even number of rotor slots that do not produce higher frequency stator-current components. From Table I, such a machine is found at $p = 2$, $S = 72$, and $R = 58$. For this machine, $R/p \pm \nu = 29 \pm \nu$, $(S - R)/p \pm \nu = 7 \pm \nu$, and $R/p \pm (\nu + 2) = 29 \pm (\nu + 2)$, i.e., all of these relationships lead to even numbers for any ν, which is, on the other side, always an odd number. Therefore, in this machine, none of the mentioned harmonics exist.

From Table I, two conclusions could be drawn.

1) First, high-speed machines, i.e., machines with one pair of poles, are very rich in high-frequency stator-current components. However, for the most common combinations of stator slot and rotor bar numbers, such machines did not develop any of "big big" harmonics. Therefore, it can be expected that such machines are quiet in operation, noise free, without high vibrations, etc., as approved in [28].
2) Second, it can be observed that the very prominent harmonics in current spectrum in motors with $p >= 2$ are saturation-related harmonics, not PSHs. As induction motors are mostly operated in partly saturated conditions, these harmonics always exist in the spectrum. This fact was not recognized anywhere in open literature before. It should be taken into account, particularly in sensorless speed controlled drives, as these harmonics are also speed (or slip or load) dependent. Tracking of such prominent harmonics in stator-current spectrum is thus much easier than tracking some of the harmonics that are not so highlighted.

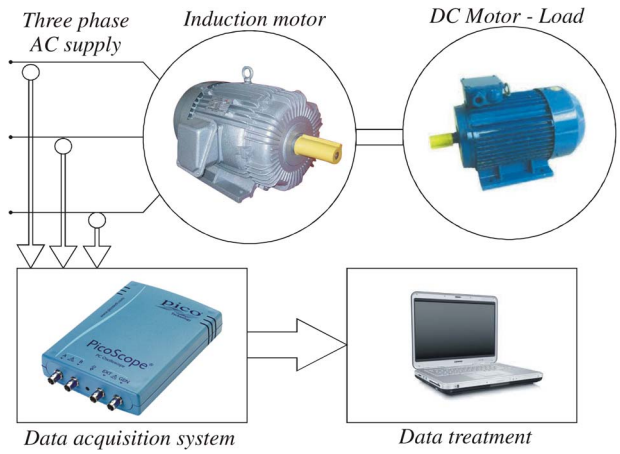

Fig. 2. Block diagram of the experimental setup.

VI. CASE STUDY

The stator-current frequency components analytically predicted earlier can be found in the measured spectrum of a cage induction machine. Measurements were thus conducted on three laboratory motors (A, B, and C), with different numbers of poles and rotor bars. The stator-current spectrum was recorded using a current clamp together with PicoScope acquisition system. Fig. 2 shows the block diagram of the experimental setup. Additionally, stator-current spectrum of a fourth motor (D) is taken from [29].

A. $p = 1$, $S = 24$, and $R = 18$

This machine is special in the sense that the current spectrum should contain both PSHs, according to (15). Experimentally recorded current spectrum clearly confirms this expectation (Fig. 3). As the current spectrum is recorded under the no-load conditions, PSH occurs at $(1 \pm R/p)f_1 = (1 \pm 18) \cdot 50$ Hz $=$ 850 and 950 Hz. Additionally, two saturation-related harmonics at $(3 \pm R/p)f_1 = (3 \pm 18) \cdot 50$ Hz $= 750$ and 1050 Hz are also observable in the spectrum. However, none of them are so prominent compared to the harmonics at 150, 250, or 350 Hz.

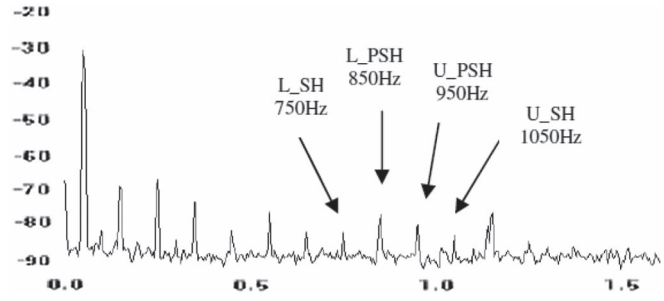

Fig. 3. Experimentally recorded stator-current spectrum for unloaded cage rotor induction motor with $S = 24$ slots, $R = 18$ bars, and $p = 1$ pole pair.

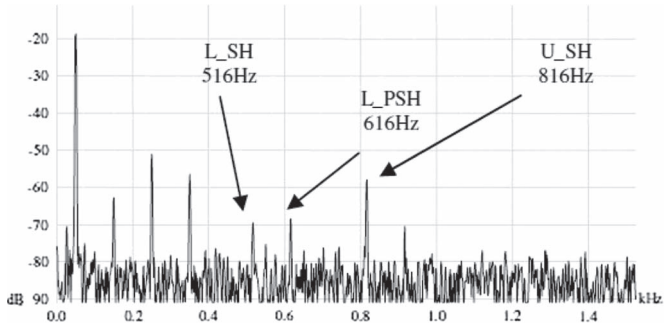

Fig. 4. Experimentally recorded stator-current spectrum for cage rotor induction motor with $S = 36$ slots, $R = 28$ bars, and $p = 2$ pole pairs at $s = 4.86\%$.

B. $p = 2$, $S = 36$, *and* $R = 28$

Fig. 4 shows experimentally obtained stator-current spectrum for an induction motor with $S = 36$ stator slots, $R = 28$ rotor bars, and $p = 2$ pairs of poles. In accordance with predictions, only lower PSH exists in the spectrum at 616 Hz, for $s = 4.86\%$. Additionally, both saturation-related current components appear in the spectrum at predicted frequencies [(39) and (40)], i.e., at 516 and 816 Hz for $s = 4.86\%$.

Moreover, saturation-related component at 816 Hz is one of the most prominent harmonics in the spectrum. This phenomenon can be easily explained. Magnetic flux density wave (36) has fundamental number of pole pairs $p = 2$ for $\nu = -17$. On the other side, stator MMF space harmonic for $\nu = -17$ is rather high because this harmonic is the stator slot harmonic ($S = 36$ and $p = 2$). Thus, these two facts cumulatively lead to rather high current component at upper saturation-related frequency.

The other saturation-related current component at 516 Hz is not so prominent because magnetic flux density wave (34) could have fundamental number of pole pairs only for $\nu = 13$, i.e., for stator MMF space harmonic of rather small magnitude.

C. $p = 2$, $S = 36$, *and* $R = 32$

Fig. 5 shows the stator-current spectrum for loaded four-pole cage rotor induction motor with $S = 36$ stator slots and $R = 32$ rotor bars at $s = 6.4\%$. Only upper PSH exists in the spectrum according to predictions. Moreover, upper PSH at 798 Hz is one of the most prominent higher harmonics in the whole stator-current spectrum. Although the fundamental rotor current of the loaded motor has a significant influence on the

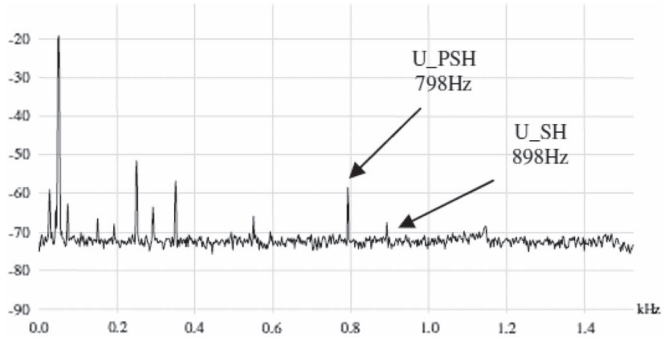

Fig. 5. Experimentally recorded stator line current spectrum for loaded cage rotor induction motor with $S = 36$ slots, $R = 32$ bars, and $p = 2$ pole pairs. Slip: $s = 6.4\%$.

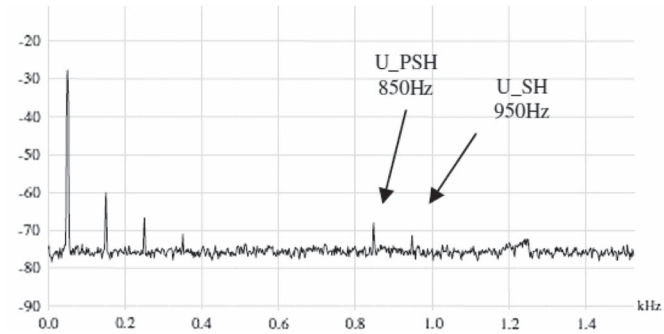

Fig. 6. Experimentally recorded stator line current spectrum for unloaded cage rotor induction motor with $S = 36$ slots, $R = 32$ bars, and $p = 2$ pole pairs.

PSH intensity, such a high PSH component can be explained only by the significant additional influence of slot permeance harmonics.

Indeed, this motor has a certain number of stator and rotor slots that the slot permeance harmonics will also have a very significant influence on the same PSH amplitude. From (21), it follows that $(S - R)/p - \nu = (36 - 32)/2 - 1 = 1$ which means that the fundamental stator MMF wave through the slot permeance produces upper PSH. Hence, it might reasonably be expected that this upper PSH is very prominent in the stator-current spectrum in no load, too. This explanation can be underpinned by stator-current spectrum in no-load condition (Fig. 6).

D. $p = 2$, $S = 36$, *and* $R = 44$

Fig. 7 depicts stator-current spectrum for a loaded 60-Hz four-pole cage rotor induction motor with $S = 36$ stator slots and $R = 44$ rotor bars [29]. Only upper PSH exists in the spectrum at 1325 Hz according to previously derived rules. Lower PSH at 1205 Hz is almost invisible. Lower saturation-related harmonic at 1085 Hz is the most prominent harmonic (denoted big big) in this part of spectra because the pole pair number of flux density wave given by (34) is equal to one of the stator slot harmonics for $\nu = 1$, i.e., $(R/p - (\nu + 2)) = (44/2 - (1 + 2)) = 19$. On the other side, for $\nu = 19$, $(R/p - (\nu + 2)) = (44/2 - 21) = 1$ Upper saturation-related harmonic at 1445 Hz is not so pronounced because the pole

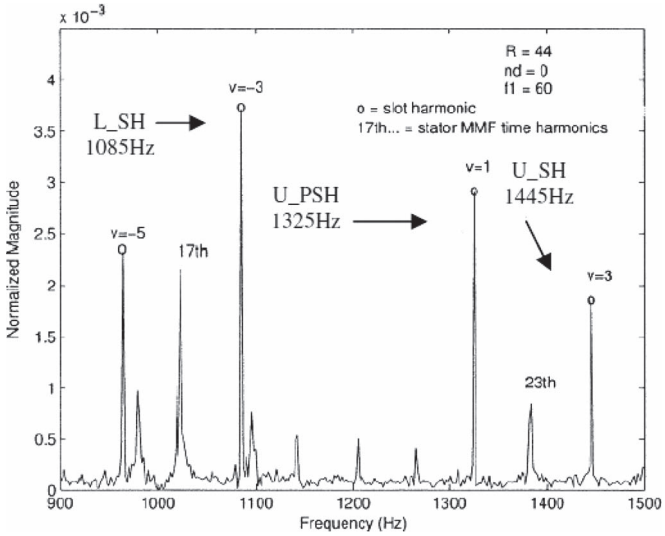

Fig. 7. Stator line current spectrum for loaded 60-Hz cage rotor induction motor with $S = 36$ slots, $R = 44$ bars, and $p = 2$ pole pairs[17]. Slip: $s = 4.16\%$.

pair numbers in flux density wave given by (36) cannot attain any significant value.

Figs. 3–7 shows also, besides the predicted, additional current components that are, on a first place, at 150, 250, and 350 Hz.

The third time harmonic (150 Hz) in a stator-current spectrum is a consequence of asymmetrical voltage supply, i.e., of some amount of inverse rotating magnetic flux wave in the air gap $\nu = -1$ in (32). Namely, none of the three-phase voltage supplies are ideally symmetrical as it is the case with real induction machine windings, too.

The existence of fifth and seventh current time harmonics is due to the voltage time harmonics in the supply voltages.

It has to be stressed that some of the PSHs that ordinarily could not exist in spectrum of healthy machine may be visible as a consequence of asymmetrical voltage supply and/or asymmetrical stator phase windings. In such cases, some amount of inverse rotating magnetic flux wave in air gap exists $\nu = -1$. Such a case can be seen, for example, at motor with $S = 36$ stator slots, $R = 32$ rotor bars, and $p = 2$. Such a motor could develop only upper PSH (14). However, for $\nu = -1$, such motor could also develop, in some amount, lower PSH as one can easily conclude from (7) where, for $\nu = -1$, the number of pole pairs in magnetic flux density wave corresponds to the 17th harmonic.

VII. Conclusion

A thorough characterization and classification of the harmonics present in a healthy cage rotor induction motor spectrum as a starting point for diagnosis of different faulty regimes using MCSA has been given in this paper. MMF space harmonics, slot permeance harmonics, and saturation of main magnetic flux path through the virtual air-gap permeance variation are taken into analytical consideration.

This paper introduces general rules which give the connection between the number of stator slots, rotor bars, and pole pairs and the existence of RSHs as well as saturation-related harmonics in the stator-current spectrum.

Saturation-related harmonics are recognized as the most prominent harmonics in cage rotor induction motors with number of pole pairs equal or greater than two, for certain combination of stator slots and rotor bars. This fact could be very interesting for use of such motors for sensorless speed tracking.

All of the predicted spectral components of the stator current are experimentally verified on different laboratory motors with different numbers of pole pairs, stator slots, and rotor bars.

References

[1] A. Bellini, F. Filippetti, C. Tassoni, and G. A. Capolino, "Advances in diagnostic techniques for induction machines," *IEEE Trans. Ind. Electron.*, vol. 55, no. 12, pp. 4109–4126, Dec. 2008.

[2] S. H. Kia, H. Henao, and G. A. Capolino, "Windings monitoring of wound rotor induction machines under fluctuating load conditions," in *Proc. IEEE IECON*, 2011, pp. 3459–3465.

[3] R. Kianinezhad, B. Nahid-Mobarakeh, L. Baghli, F. Betin, and G. A. Capolino, "Modeling and control of six-phase symmetrical induction machine under fault condition due to open phases," *IEEE Trans. Ind. Electron.*, vol. 55, no. 5, pp. 1966–1977, May 2008.

[4] K.-H. Kim, "Simple online fault detecting scheme for short-circuited turn in a PMSM through current harmonic monitoring," *IEEE Trans. Ind. Electron.*, vol. 58, no. 6, pp. 2565–2568, Jun. 2011.

[5] L. Cappochi, S. Toma, G. A. Capolino, F. Fnaiech, and A. Yazidi, "Wound-rotor induction generator short-circuit fault classification using a new neural network based on digital data," in *Proc. SDEMPED*, 2011, pp. 638–644.

[6] L. Saidi, H. Henao, F. Fnaiech, G. A. Capolino, and G. Cirrincione, "Application of higher order spectral analysis for rotor broken bar detection in induction machines," in *Proc. SDEMPED*, 2011, pp. 31–38.

[7] T. M. Wolbank, P. Nussbaumer, H. Chen, and P. E. Macheiner, "Monitoring of rotor-bar defects in inverter-fed induction machines at zero load and speed," *IEEE Trans. Ind. Electron.*, vol. 58, no. 5, pp. 1468–1478, May 2011.

[8] M. Blodt, D. Bonacci, J. Regnier, M. Chabert, and J. Faucher, "On-line monitoring of mechanical faults in variable-speed induction motor drives using the Wigner distribution," *IEEE Trans. Ind. Electron.*, vol. 55, no. 2, pp. 522–533, Feb. 2008.

[9] C. Bruzzese and G. Joksimović, "Harmonic signatures of static eccentricities in the stator voltages and in the rotor current of no-load salient-pole synchronous generators," *IEEE Trans. Ind. Electron.*, vol. 58, no. 5, pp. 1606–1624, May 2011.

[10] R. N. Andriamalala, H. Razik, L. Baghli, and F. M. Sargos, "Eccentricity fault daignosis of a dual-stator winding induction machine drive considering the slotting effects," *IEEE Trans. Ind. Electron.*, vol. 55, no. 12, pp. 4238–4251, Dec. 2008.

[11] V. Choqueuse, M. E. L. Benbouzid, Y. Amirat, and S. Turri, "Diagnosis of three-phase electrical machines using multidimensional demodulation techniques," *IEEE Trans. Ind. Electron.*, vol. 59, no. 4, pp. 2014–2023, Apr. 2012.

[12] S. Nandi, T. C. Ilamparithi, S. B. Lee, and D. Hyun, "Detection of eccentricity faults in induction machines based on nameplate parameters," *IEEE Trans. Ind. Electron.*, vol. 58, no. 5, pp. 1673–1683, May 2011.

[13] D. Morinigo-Sotelo, L. A. Garcia-Escudero, O. Duque-Perez, and M. Perez-Alonso, "Practical aspects of mixed-eccentricity detection in PWM voltage-source-inverter-fed induction motors," *IEEE Trans. Ind. Electron.*, vol. 57, no. 1, pp. 252–262, Jan. 2010.

[14] M. A. Rodriguez-Blanco, A. Claudio-Sanchez, D. Theilliol, L. G. Vela-Valdes, P. Sibaja-Teran, L. Hernandez-Gonzalez, and J. Aguayo-Alquicira, "A failure-detection strategy for IGBT based on gate-voltage behavior applied to a motor drive system," *IEEE Trans. Ind. Electron.*, vol. 58, no. 5, pp. 1625–1633, May 2011.

[15] P. Lezana, J. Pou, T. A. Meynard, J. Rodriguez, S. Ceballos, and F. Richardeau, "Survey on fault operation on multilevel inverters," *IEEE Trans. Ind. Electron.*, vol. 57, no. 7, pp. 2207–2218, Jul. 2010.

[16] S. Nandi, H. A. Toliyat, and X. Li, "Condition monitoring and fault diagnosis of electrical motors—A review," *IEEE Trans. Energy Convers.*, vol. 20, no. 4, pp. 719–729, Dec. 2005.

[17] J. H. Jung, J. J. Lee, and B. H. Kwon, "Online diagnosis of induction motors using MCSA," *IEEE Trans. Ind. Electron.*, vol. 53, no. 6, pp. 1842–1852, Dec. 2006.
[18] G. Joksimović, J. Riger, T. Wolbank, N. Perić, and M. Vašak, "Stator line current spectrum content of a healthy cage rotor induction machine," in *Proc. SDEMPED*, Bologna, Italy, Sep. 2011, pp. 113–118.
[19] S. Nandi, "Modeling of induction machines including stator and rotor slot effects," *IEEE Trans. Ind. Appl.*, vol. 40, no. 4, pp. 1058–1065, Jul./Aug. 2004.
[20] S. Williamson and Y. N. Feng, "Slot-harmonic fields in closed-slot machines," *IEEE Trans. Ind. Appl.*, vol. 44, no. 4, pp. 1165–1171, Jul./Aug. 2008.
[21] S. Nandi, "A detailed model of induction machines with saturation extendable for fault analysis," *IEEE Trans. Ind. Appl.*, vol. 40, no. 5, pp. 1302–1309, Sep./Oct. 2004.
[22] T. Jokinen and V. Hrabovcova, *Design of Rotating Electrical Machines*. Hoboken, NJ: Wiley, 2009.
[23] G. Joksimović, M. Đurović, and J. Penman, "Cage rotor MMF—Winding function approach," *IEEE Power Eng. Rev.*, vol. 21, no. 4, pp. 64–66, Apr. 2001.
[24] Z. Gao, T. G. Habetler, R. G. Harley, and R. S. Colby, "A sensorless rotor temperature estimator for induction machines based on a current harmonic spectral estimation scheme," *IEEE Trans. Ind. Electron.*, vol. 55, no. 1, pp. 407–416, Jan. 2008.
[25] X. R. Kiani, F. Betin, V. Lanfranchi, A. Yazidi, and G. A. Capolino, "Intelligent sensorless speed control of six-phase induction machine," in *Proc. IECON*, 2011, pp. 4198–4203.
[26] S. H. Kia, H. Henao, and G. A. Capolino, "Some digital signal processing techniques for induction machines diagnosis," in *Proc. SDEMPED*, 2011, pp. 322–329.
[27] G. Joksimović, "Line current spectrum analysis in saturated three-phase cage induction machine," *Elect. Eng.*, vol. 91, no. 8, pp. 425–437, Apr. 2010.
[28] B. Cassoret, J. P. Lecointe, and J. F. Brudny, "Influence of the pole number on the magnetic noise of electrical ac machines," *Progr. Electromagn. Res. B*, vol. 33, pp. 83–97, 2011.
[29] K. Kim, A. G. Parlos, and R. M. Bharadwaj, "Sensorless fault diagnosis of induction motors," *IEEE Trans. Ind. Electron.*, vol. 50, no. 5, pp. 1038–1051, Oct. 2003.

Gojko M. Joksimović (M'98–SM'11) received the Ph.D. and Full Professor degrees from the University of Montenegro, Podgorica, Montenegro, in 2000 and 2011, respectively.

He is with the Faculty of Electrical Engineering, University of Montenegro. His main research areas include analysis of electrical machines, condition monitoring of electrical machines, and power electronics and control. He is the author of a few books and more than 50 papers published in leading international scientific journals and international conference proceedings.

Jakša Riger received the B.Sc. degree from the Faculty of Electrical Engineering, University of Montenegro, Podgorica, Montenegro, in 2011.

He is with the Faculty of Electrical Engineering, University of Montenegro. His research interests are analysis of electrical machines and condition monitoring of electrical machines.

Thomas M. Wolbank (M'92) received the Doctoral and Associate Professor degrees from Vienna University of Technology, Vienna, Austria, in 1996 and 2004, respectively.

He is currently with the Institute of Energy Systems and Electrical Drives, Department of Electrical Drives and Machines, Vienna University of Technology. He has coauthored some 100 papers in refereed journals and international conference proceedings. His research interests include saliency-based sensorless control of ac drives, dynamic properties and condition monitoring of inverter-fed machines, and transient electrical behavior of ac machines.

Nedjeljko Perić (M'94–SM'04) received the B.Sc., M.Sc., and Ph.D. degrees in electrical engineering from the Faculty of Electrical Engineering and Computing (FER), University of Zagreb (UNIZG), Zagreb, Croatia, in 1973, 1980, and 1989, respectively.

From 1973 to 1993, he was with the Institute of Electrical Engineering, Končar Corporation, Zagreb, as an R&D Engineer, the Head of the Positioning Systems Department, and the Manager of the Automation Section. Since 2010, he has been the Dean of the Faculty of Electrical Engineering and Computing (FER), University of Zagreb (UNIZG), where he joined the Department of Control and Computer Engineering as an Associate Professor in 1993 and was appointed as a Full Professor in 1997. His current research interests are in the fields of process identification and advanced control techniques.

Mario Vašak (M'07) received the Ph.D. degree in electrical engineering from the Faculty of Electrical Engineering and Computing (FER), University of Zagreb (UNIZG), Zagreb, Croatia, in 2007.

He is an Assistant Professor with the Department of Control and Computer Engineering, Faculty of Electrical Engineering and Computing (FER), University of Zagreb (UNIZG). He works in the areas of predictive/robust/fault-tolerant control. He has published over 40 papers in journals and conference proceedings.